INTERFACE

rsif.royalsocietypublishing.org

Research

Cite this article: Riehl BD, Lee JS, Ha L, Lim JY. 2015 Fluid-flow-induced mesenchymal stem cell migration: role of focal adhesion kinase and RhoA kinase sensors. *J. R. Soc. Interface* **12**: 20141351.
http://dx.doi.org/10.1098/rsif.2014.1351

Received: 10 December 2014
Accepted: 16 December 2014

Subject Areas:
bioengineering

Keywords:
stem cell migration, fluid shear, focal adhesion kinase, RhoA kinase, time lapse

Author for correspondence:
Jung Yul Lim
e-mail: jlim4@unl.edu

THE ROYAL SOCIETY
PUBLISHING

Fluid-flow-induced mesenchymal stem cell migration: role of focal adhesion kinase and RhoA kinase sensors

Brandon D. Riehl[1], Jeong Soon Lee[1], Ligyeom Ha[1] and Jung Yul Lim[1,2]

[1]Department of Mechanical and Materials Engineering, University of Nebraska-Lincoln, Lincoln, NE 68588, USA
[2]The Graduate School of Dentistry, Kyung Hee University, Seoul, Korea

The study of mesenchymal stem cell (MSC) migration under flow conditions with investigation of the underlying molecular mechanism could lead to a better understanding and outcome in stem-cell-based cell therapy and regenerative medicine. We used peer-reviewed open source software to develop methods for efficiently and accurately tracking, measuring and processing cell migration as well as morphology. Using these tools, we investigated MSC migration under flow-induced shear and tested the molecular mechanism with stable knockdown of focal adhesion kinase (FAK) and RhoA kinase (ROCK). Under steady flow, MSCs migrated following the flow direction in a shear stress magnitude-dependent manner, as assessed by root mean square displacement and mean square displacement, motility coefficient and confinement ratio. Silencing FAK in MSCs suppressed morphology adaptation capability and reduced cellular motility for both static and flow conditions. Interestingly, ROCK silencing significantly increased migration tendency especially under flow. Blocking ROCK, which is known to reduce cytoskeletal tension, may lower the resistance to skeletal remodelling during the flow-induced migration. Our data thus propose a potentially differential role of focal adhesion and cytoskeletal tension signalling elements in MSC migration under flow shear.

1. Introduction

Mesenchymal stem cells (MSCs) play a key role in tissue homeostasis and repair. MSCs migrate from niches in the body to the tissues that are damaged or to be remodelled, and after arrival they undergo tissue-specific commitment and differentiation and release growth factors to facilitate regeneration [1,2]. Migrating MSCs are exposed to fluid-flow-induced shear in the vasculature. The shear stresses cells experience in the vasculature vary with location, heart rate and many other factors. Arteries typically have wall stresses in the range of 10–70 dyne cm^{-2}, and veins have lower stresses of 1–6 dyne cm^{-2} [3]. While it has been recognized that flow shear stress stimulation influences various MSC functions [4,5], very little is known regarding the role of flow shear in affecting MSC migration. Understanding how MSCs migrate under fluid flow, for both the *in vitro* expanded culture and the *in vivo* situation, could significantly improve MSC-based cell therapy and regenerative medicine outcomes [6].

In this study, we developed methods for accurately tracking and measuring cell migration and morphology for both static and flow conditions. Our methods used peer-reviewed open source cell tracking software and added the ability to measure cell morphology changes, process tracking data and manage multiple datasets. Our method is able to remove the microscope stage drift via using FIJI (biological image analysis tool [7]) and to perform the pre-processing, segmentation, and automated tracking using an open source peer-reviewed time lapse analyser (TLA [8]). We wrote a custom Matlab program to measure cell morphology, analyse the tracking data from TLA and perform other calculations relevant to the experiment (the codes will be available upon request). Our program allows the user to select which cells are used in measurement and

calculation. It also manages datasets for multiple conditions and experimental runs and is able to plot, animate and perform statistical tests of the obtained data. Although we chose to use TLA for cell tracking, our program can also open output files from MTrack2 and other similar formats.

Most cell migration studies have assessed cell movement under static culture conditions and have primarily tested the effects of biochemical cell-migration-driving factors such as chemokines [9]. However, it is increasingly recognized that other cues than chemokine concentration gradient, such as static and dynamic mechanical cues or electric fields, also play a critical role in cell migration [10]. We investigated MSC migration under fluid flow mechanical conditions with the rationale described above. Cells under flow-induced shear may react through various molecular sensors [11]. Integrin-mediated focal adhesion and cytoskeletal structures anchored to it are likely to be the primary sites that resist fluid shear, and may provide a mechanism through which migration traction force is exerted. Focal adhesion kinase (FAK) is a key focal adhesion signalling molecule and it is involved in the regulation of mechanical homeostasis and other processes such as growth and differentiation [12]. Specific to migration, FAK may play an important role because it controls cellular adhesion and spreading [13]. The control of cell migration by FAK has been specifically explored in cancer cell metastasis based on significant FAK overexpression observed in primary and metastatic tumours [14]. RhoA kinase (ROCK), the first downstream effector of Rho GTPases, is involved in actin filament formation, cytoskeletal tension-mediated cell morphology change and the resultant cell fate decision [15]. In migration, ROCK is thought to aid in the cell contraction process and may regulate transmigration through other cell layers [16]. ROCK has also been proposed to be a therapeutic target for disorders of the central nervous system, because inhibiting ROCK enhanced neural cell elongation, protrusion and migration [17]. While the role of FAK and ROCK, molecular elements each representing key focal adhesion and cytoskeletal tension signalling cascades, in cell migration has been suggested, there is limited information regarding their control of cell migration under flow shear, especially for MSCs.

Using the developed methods for cell tracking, measurement and processing, we examined the effects of flow-induced shear stress on C3H10T1/2 murine MSC migration and morphology. Cells were subjected to physiologically relevant shear stresses at 2, 15 and 25 dyne cm^{-2} (labelled FF2, FF15 and FF25, respectively), and time lapse microscopy data were collected, analysed and compared with those of unflowed static control. To test the molecular mechanism of MSC migration under flow, MSCs with stable FAK and ROCK-I silencing were established using the small hairpin RNA (shRNA) technique and cell responses under flow were compared with those of vector control cells.

2. Material and methods

2.1. Small hairpin RNA

Establishing MSCs with stable FAK or ROCK knockdown has been previously reported [18,19]. Briefly, murine C3H10T1/2 MSCs (ATCC, CCL-226) were transfected for 24 h with shRNA–FAK (sc-35353-SH) or shRNA–ROCK-I (sc-36432-SH), both from Santa Cruz Biotechnology, using lipofectamine 2000 (Invitrogen) transfection reagent. The cells were then exposed to the selection media containing 2 μg ml^{-1} puromycin. The puromycin-resistant cells were selected for further passaging to establish stable knockdown cells. Vector control was produced by repeating the procedure but with green fluorescent protein (GFP) control plasmid (Santa Cruz Biotechnology, sc-108083). Silencing of FAK and ROCK was confirmed by RT-PCR and immunoblotting [18,19]. Examples of Western blotting data for silenced FAK and ROCK are shown in the electronic supplementary material, figure S14. In contrast to small interference RNA exerting only a transient silencing, shRNA adopted, in this study, allows high potency and sustainable interference and less off-target silencing via endogenous machinery [20]. The sustainable interference was checked with immunoblotting after subcultures.

2.2. Cell culture

Cells were cultured in growth media composed of Dulbecco's modified Eagle medium supplemented with 10% fetal bovine serum (FBS), 1% penicillin–streptomycin and 2 μg ml^{-1} puromycin. Glass slides (75 × 25 mm^2, thickness of 1 mm), which fit to the flow chamber, were sterilized by exposure to UV light for 2 h. Cells were seeded at 1×10^5 cells in 1 ml of media per slide. After allowing adhesion for 1 h, the media were changed to the serum-reduced media (with 5% FBS), in which cells were kept overnight before starting the time lapse flow experiments the next day. The cell attachment number was retro-calculated by counting the unattached floating cells after 1 h of adhesion. A total of five slides for each cells (vector control, FAK–shRNA, ROCK–shRNA) were tested for adhesion.

2.3. Fluid flow set-up

The fluid flow system (Flexcell International) consists of a media reservoir, a Masterflex L/S peristaltic pump, an Osci-Flow controller, two pulse dampeners and a FlexFlow shear stress chamber (figure 1). The components were connected with Masterflex L/S 16 tubing. The media reservoir was placed in a 37°C water bath. The StreamSoft v. 4.1 software (Flexcell International) controlled the pump and flow controller. It determines the required flow rate for a given shear stress by taking into account the device dimensions, the tubing size and the media viscosity (electronic supplementary material, table S7). The shear stress experienced by the cells is assumed to be the wall shear stress.

The FlexFlow chamber, which enables *in situ* observation of the cells under fluid flow, was assembled as directed by the manufacturer. The flow system was sterilized by 10 min of flow with 70% ethanol through the tube and then flushed with deionized water twice. The water was drained, and then 400 ml of flow media (the same serum-reduced media with 5% FBS) was added to the reservoir. The media were circulated until all air bubbles were removed from the system. For flow experiments, a slide seeded with cells was placed in the FlexFlow device, and the vacuum was applied to hold the slide. The vacuum seal was checked for leaks before placing the FlexFlow on the inverted microscope. The device was held by the microscope stage and secured with laboratory tape. To avoid air entrapment in the system owing to each slide assembling, the media were primed after every slide change for 30 s. This could prevent bubbles from shearing off the cells. The fluid flow stimulation of cells was performed for 2 h at three different shear stresses (2, 15 and 25 dyne cm^{-2}) under steady flow conditions. The static unflowed control was observed using the same FlexFlow chamber but without fluid shear. At least four different flow experiments were performed for each condition.

2.4. Time lapse imaging

A section of the cell-cultured slide away from the edges and containing at least 10 free cells was selected for imaging. Cells

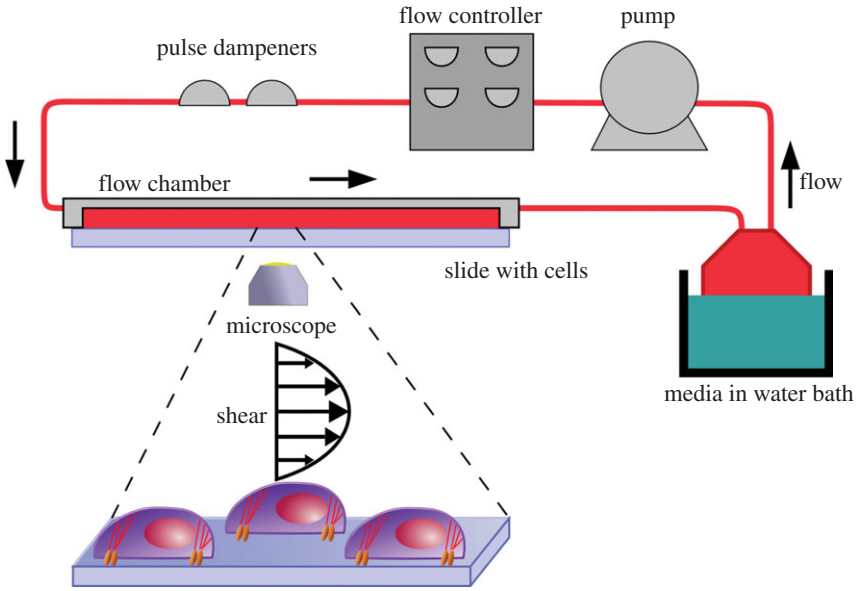

Figure 1. Schematic of the fluid flow set-up. The cell-seeded glass slide was assembled with the FlexFlow chamber and placed on the inverted microscope for time lapse imaging. Steady flows at 2, 15 and 25 dyne cm^{-2} shear stress were applied, and cell migration and morphology were measured using our program.

clumped or interconnected were excluded in the processing. The time lapse recording of phase contrast images was conducted once per minute up to 2 h with a Leica inverted microscope at 10× magnification using the Leica application suite software.

2.5. Image processing

The first step in the image processing was to remove motion owing to microscope stage drift and slide movement. This was adopted from FIJI, which used the template matching plugin [7]. A template was selected for each phase contrast image stack from a region of the background that contained distinguished features. All subsequent images in the stack were aligned to this template. The transform coordinates from the phase contrast stacks were used in a Matlab script to align the image stacks. The contrast was adjusted using the automatic window/level feature in FIJI.

The stabilized image stacks were processed to detect cell outlines in TLA. Two separate binary masks were created and added. One mask was created by applying the Otsu threshold to the image entropy. The second mask was created using Sobel edge detection. These two masks combined (electronic supplementary material, figure S1) could consistently detect the cell outlines. The binary mask images were then used for automated cell tracking and for cell morphology measurements. See the electronic supplementary material, tables S9–S11 for the full mask creation details. Video examples of time-series cell migration tracks can be found in the electronic supplementary material, information section, and examples of captured time-series images of the cells are shown in the electronic supplementary material, figure S2.

2.6. Data processing

Automated cell tracking was performed in the TLA and the morphology measurement, data processing and statistics were performed in our custom Matlab script. See the electronic supplementary material, information section for the cell tracking details and measurement descriptions.

2.7. Statistics

Statistical significance was tested using one-way analysis of variance (ANOVA) with a Tukey–Kramer *post hoc* test in Matlab. The data were checked to ensure the ANOVA assumptions were met (electronic supplementary martial, information). Skewed data were detected by plotting the residuals of ANOVA against a standard normal curve. A $\log_{10}$ transform was applied to the skewed data before applying statistical tests, which were then back-transformed. The back-transformed mean becomes the geometrical mean, and the confidence intervals become asymmetric. The data are presented as mean ± standard error of measurement (SEM). The symbols in the figures that mark statistical significance compared with static control, FF2, FF15, FAK–shRNA static and ROCK–shRNA static are *, #, Ψ, ‡ and +, respectively. The *p*-values less than 0.05, 0.01 and 0.001 are indicated by single, double and triple symbols, respectively.

3. Results

3.1. Fluid shear directs mesenchymal stem cell migration in a shear stress-dependent manner

The cell outline was detected (electronic supplementary material, figure S1) using the developed masks, from which the cell centroid position at each time frame was determined. Cell migration raw track data under static and flow conditions could be obtained by connecting the centroids (figure 2*a*; each coloured line represents each cell movement for 2 h adjusted to begin from the centre of the plot; for fluid flow samples, flow was applied horizontally from left to right; also see videos in the electronic supplementary material, information). The compass plot (figure 2*b*) and rose plot (figure 2*c*) could be obtained from the raw tracks to show total displacement and angular histograms, respectively. It could be seen from these plots that sheared MSCs travelled following the flow direction (from left to right). In quantification based on the migration angle criteria (figure 2*d*), the percentage of cells migrating with the flow showed an increasing trend with the shear stress magnitude applied (figure 2*e*). The percentage of time that cells migrated with the flow direction was significantly increased in the FF25 condition compared with unflowed static control and FF2 and FF15 (figure 2*f*). The time spent migrating against the flow direction appeared to have a decreasing trend at higher shear stresses, but did not reach statistical significance.

Analyses using our program could further provide multi-aspect information on cell migration. The average total

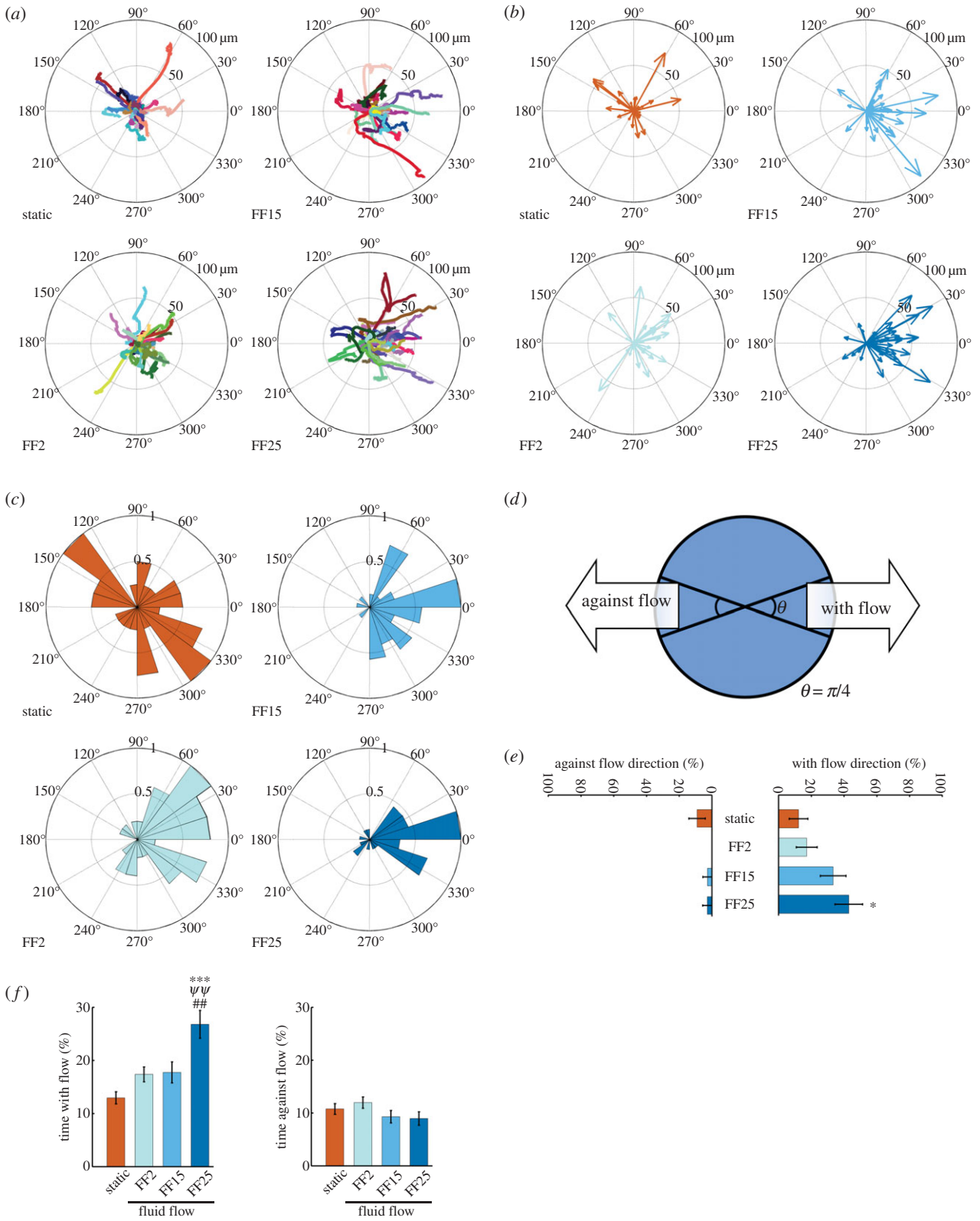

Figure 2. Fluid shear induces MSC migration in the flow direction. (*a*) Raw cell migration tracks. The individual cell tracks are distinguished by colour. Each track start was equalized to the centre of the plot. The concentric rings mark 50 and 100 μm from the centre. Fluid flow (FF) figures are presented with the flow direction horizontal from left to right. (*b*) Compass plots displaying total displacement and migration direction. (*c*) Rose plots displaying a normalized angular histogram of the cell migration angles. (*d*) A cell having a migration angle within $\pm\pi/8$ of the flow direction was defined as a cell migrating with the flow. The opposite was defined as migrating against the flow. (*e*) The percentage of cells migrating with the flow quantified based on the criteria in panel (*d*) showed an increasing trend with shear stress. (*f*) The percentage of time the cells spent migrating with the flow quantified on the basis of the criteria in panel (*d*) increased with shear stress. All the data are presented as the mean with SEM. $^{*}p < 0.05$ and $^{***}p < 0.001$ compared with unflowed static control. $^{\#\#}p < 0.01$ compared with FF2. $^{\Psi\Psi}p < 0.01$ compared with FF15.

displacement increased with shear stress, giving significantly longer migration at FF25 compared with static control and FF2 (figure 3*a*). The confinement ratio, a measure of the directness of the migration path, followed a similar increasing trend with shear stress (figure 3*b*). The arrest coefficient, measuring the percentage of time a cell is paused, was not

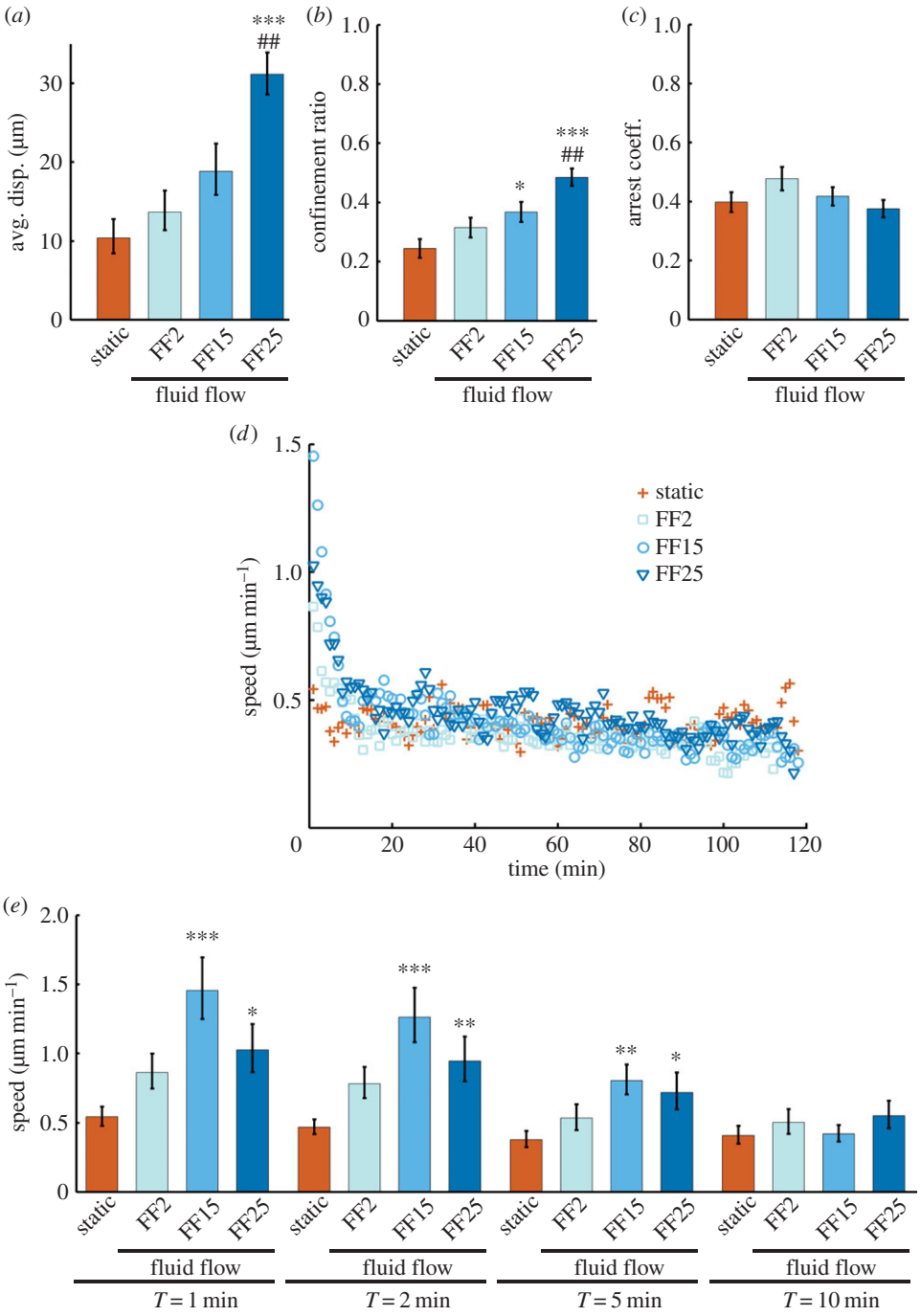

Figure 3. Flow shear increases displacement and efficiency of migration path. (*a*) The average total displacement had an increasing trend with increasing shear stress. (*b*) The confinement ratio, quantifying how direct the migration path is, also increased with shear stress. (*c*) The arrest coefficient, the percentage of time the cells are paused, was not statistically different. (*d*) The cell speed for each cell in each frame was measured, from which the average speed of the cells as a timeseries was plotted. FF groups showed peak cell speeds with the start of the flow. (*e*) Cell speeds of the FF15 and FF25 groups were significantly greater than the static control for the first 5 min. The bar graphs are presented as the mean with SEM. Static control, plus symbol; FF2, squares; FF15, circles; FF25, inverted triangle. *, ** and ***$p < 0.05$, 0.01 and 0.001 compared with the static control, respectively. $^{\#\#}p < 0.01$ compared with FF2.

significantly different among conditions (figure 3*c*). Taken together, flow shear induced MSCs to travel further following the flow direction in a straighter path.

The cellular speed at each interval could also be calculated (figure 3*d*). Unflowed cells (static) showed no marked changes in cell speed up to 2 h. Interestingly, flowed cells displayed a peak speed with an onset of the flow. The FF2, FF15 and FF25 groups showed, respectively, an average peak speed of 0.86, 1.45 and 1.02 $\mu m\ min^{-1}$ (figure 3*d*,*e*, 1 min), which were greater than the mean speed (0.54 $\mu m\ min^{-1}$) of the unflowed cells averaged for 2 h. However, after the peak, the cell speed decreased with a continuation of the flow, and there were no significant differences among test conditions after about 10 min of flow. It is notable that FF15 induced the highest average peak speed (higher than FF25). This suggests that transient cell responsiveness to flow may be maximized at some optimal shear level. On the other hand, cell migration parameters cumulated for the entire time lapse period (figures 2*e*,*f*, 3*a*,*b* and 5*i*) exhibited rather monotonous changes with shear stress. The increase in displacement with shear may have resulted from the interplay of cell speed, confinement ratio and arrest coefficient.

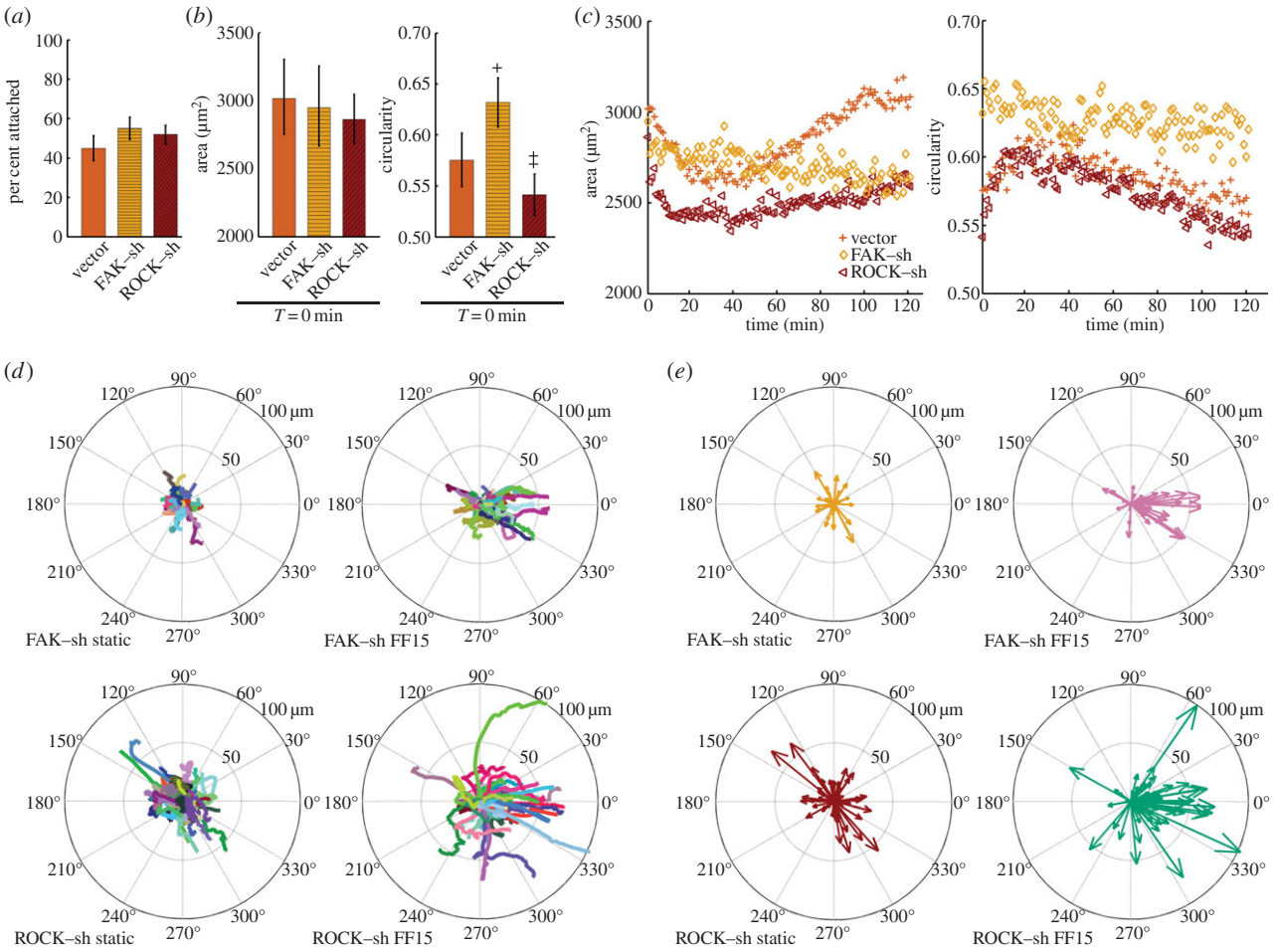

Figure 4. Silencing FAK suppresses migration and morphology adaptation, whereas ROCK interference facilitates migration. (*a*) Cell seeding efficiency was not significantly different among the cells. (*b*) Initial cell area was not statistically different but slightly less for silenced cells. Initial cellular circularity was significantly greater for FAK–shRNA than for ROCK–shRNA. (*c*) The timeseries of the area and circularity under static condition. Vector control and ROCK-silenced cells showed initial adaptation and recovery responses unlike FAK-silenced cells. (*d*) Raw migration tracks for silenced cells without and with flow at 15 dyne cm^{-2}. Fluid flow was applied horizontally from left to right. FAK–shRNA reduced cell migration while ROCK–shRNA stimulated. (*e*) Corresponding compass plots. The bar graphs are presented as the mean with SEM. Vector control static, plus; FAK–shRNA static, diamond; ROCK–shRNA static, left inverted triangle. $^{\ddagger}p < 0.05$ compared with FAK–shRNA. $^{+}p < 0.05$ compared with ROCK–shRNA.

3.2. Focal adhesion kinase and RhoA kinase silencing affects mesenchymal stem cell shape and motility under static condition

We previously reported the establishment and characterization of MSCs with stable interference of FAK [18] and ROCK [19] accomplished via shRNA. Note that all of the non-silenced cells used in this study are GFP-loaded vector control cells, including the cells used for assessing shear stress effects (figures 2 and 3). Comparisons of vector control and shRNA are shown in figures 4 and 5. As basal data, there was no significant difference in cell seeding efficiency among the cell lines (figure 4*a*). Adhered cell area was slightly less for silenced cells, whereas the circularity was significantly greater for FAK-silenced MSCs when compared with MSCs with ROCK–shRNA (figure 4*b*).

Cells displayed shape changes during the time lapse period even under static conditions. This may possibly be a response to the brief circulation of media in the chamber to remove air bubbles before the experiment. Vector control cells and ROCK-silenced MSCs had an initial area contraction followed by a gradual return towards the original area under no flow conditions (figure 4*c*). However, MSCs with FAK–shRNA did not exhibit notable area changes for the 2 h period, indicating that FAK knockdown may have disabled morphological adaptation capability. Similar results were obtained for circularity under static conditions (figure 4*c*), i.e. an initial increase then decrease for vector control and ROCK–shRNA, but no notable change for FAK–shRNA.

FAK and ROCK silencing also affected MSC motility under static conditions. MSCs with FAK–shRNA were less mobile giving a decreased displacement, whereas ROCK-silenced MSCs showed increased mobility (static cases in figures 4*d*,*e* and 5*a*). MSCs with FAK–shRNA also migrated with relatively less direct paths (static cases in figure 5*b*). Both the comparisons of the total displacement and confinement ratio between FAK–shRNA and ROCK–shRNA under static conditions reached statistical significance (figure 5*a*,*b*). The rose plot corresponding to figure 4*d* is shown in the electronic supplementary material, figure S5.

3.3. Flow-induced mesenchymal stem cell migration is differentially affected by focal adhesion kinase and RhoA kinase

As in figures 2 and 3, the FF25 group had, in general, more migration stimulatory effects among shear stresses tested. We

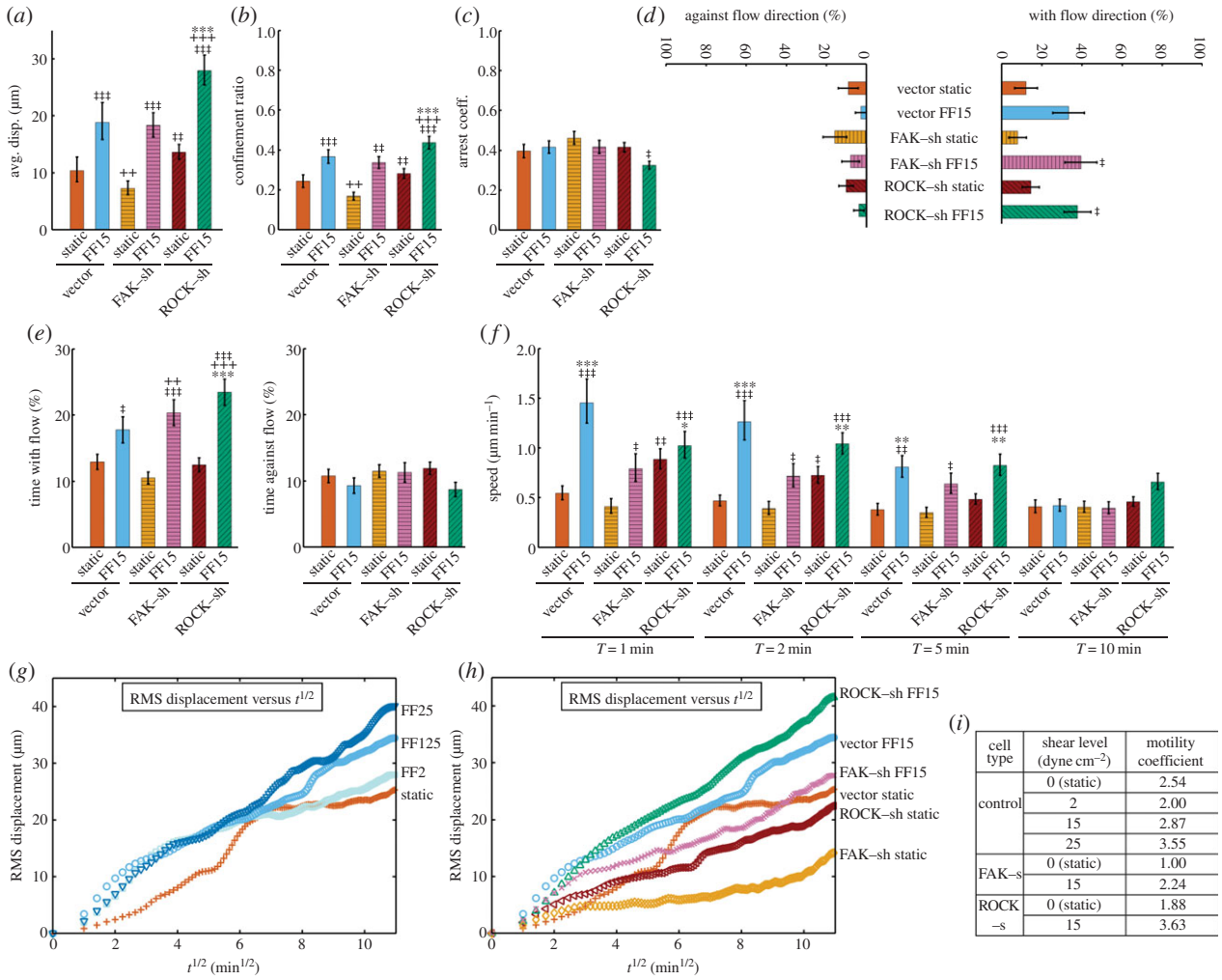

cell type	shear level (dyne cm^{-2})	motility coefficient
control	0 (static)	2.54
	2	2.00
	15	2.87
	25	3.55
FAK–s	0 (static)	1.00
	15	2.24
ROCK –s	0 (static)	1.88
	15	3.63

Figure 5. FAK silencing decreases RMS displacement and motility coefficient, whereas ROCK silencing increases them especially under flow conditions. (*a*) MSCs with ROCK−shRNA had an increased total cell displacement. (*b*) The confinement ratio showed a similar increase for ROCK−shRNA. (*c*) No significant changes were detected for the arrest coefficient other than a lower value for ROCK−shRNA than for FAK−shRNA. (*d*) Silenced cells still showed preferred migration along the flow direction. (*e*) ROCK-silenced cells under flow spent significantly more time migrating with the flow direction. (*f*) Silenced cells also showed a peak speed after the flow onset. (*g*) RMS displacement plotted against square root of time showed shear stress-dependent increases. (*h*) In the same type of plot, FAK−shRNA decreased RMS displacement for both static and flow conditions. ROCK interference increased RMS displacement especially under flow conditions. (*i*) Calculated motility coefficient increased with increasing shear stress. It had lower values for FAK−shRNA for both static and shear conditions relative to vector control counterparts. MSCs with ROCK−shRNA at FF15 exhibited the greatest motility coefficient among test conditions. The bar graphs are presented as the mean with SEM. Static control, plus; FF2, square: FF15, circle; FF25, inverted triangle; FAK−shRNA static, diamond; FAK−shRNA FF15, multiplication symbol; ROCK−shRNA static, left inverted triangle; ROCK−shRNA FF15, delta symbol. *, ** and ***: $p < 0.05$, 0.01, and 0.001 compared with vector control static. ‡, ‡‡ and ‡‡‡: $p < 0.05$, 0.01 and 0.001 compared with FAK−shRNA static. ++ and +++: $p < 0.01$ and 0.001 compared with ROCK−shRNA static.

observed, however, that more cells were washed away by the flow in the FF25 group. In testing the role of FAK and ROCK in flow-induced MSC migration, we thus chose a shear of 15 dyne cm^{-2}. Even in the presence of FAK knockdown, FF15 could still induce cell migration (comparison between static and FF15 for FAK−shRNA samples, figure 5*a*,*b*,*d*,*e*). Interestingly, silencing ROCK stimulated MSC mobility under shear stress conditions. MSCs with ROCK−shRNA under FF15 showed the greatest total displacement, confinement ratio and time migrating with the flow and had the smallest arrest coefficient (figure 5*a*–*c*,*e*), indicating that ROCK-silenced MSCs under flow tended to move further in straighter paths complying with the flow, potentially with fewer stops. Silenced cells also showed a peak speed after the flow onset (figure 5*f*). MSCs with FAK−shRNA had a lower peak speed under FF15 relative to the sheared vector control at FF15. For ROCK-silenced cells, although most of the migration parameters were increased as described above, the peak speed was relatively lower. Again, after about 10 min, there were no notable differences in cell speed among conditions.

To assess cell migration in a more collective manner, the root mean square (RMS) displacement, a measure of group dispersion, was quantified (equation 1, electronic supplementary material, information). The RMS displacement is a more holistic measure of migration that contains elements of displacement, speed, confinement and arrest of participating cells. Further, from the plot of RMS displacement versus square root of time (figure 5*g*,*h*), the motility coefficient can be determined as the average slope. The motility coefficient implies the strength of migration in the same context with the diffusion coefficient of the first-order diffusion kinetics [21]. Our data showed that with increasing stress cells displayed increasing trends in RMS displacement (figure 5*g*) and motility coefficient (figure 5*i*). MSCs with FAK−shRNA under static conditions

had a very low RMS displacement (figure 5*h*) and motility coefficient. Importantly, while shear could still induce migration for FAK-silenced cells, the RMS displacement and motility coefficient for FAK–shRNA at FF15 were decreased relative to the vector control under FF15 (figure 5*h*,*i*). This indicates that FAK silencing suppressed MSC responsiveness in migration to shear. On the other hand, silencing ROCK resulted in a remarkable increase in MSC motility especially under flow. MSCs with ROCK–shRNA at FF15 had the greatest RMS displacement and motility coefficient among all of the conditions tested (figure 5*h*,*i*), including the comparison with vector control at FF15 (and also FF25). Note that we analysed the RMS displacement as a representative measure of cell migration tendency, from which a clear correlation between flow shear and cell migration and the role of FAK and ROCK could be illustrated (figure 5*g*–*i*). We further performed an alternative migration calculation, i.e. mean square displacement (MSD) measurement. The RMS calculation uses ensemble averaging, whereas the MSD calculation uses the ensemble and time averaging (equation 2, the electronic supplementary material, information). The MSD calculation provided similar results on the flow shear control of MSC migration and its mediation by FAK and ROCK (plots of MSD are shown in the electronic supplementary material, information section and figure S8).

The time-series changes of various morphology parameters (area, circularity, orientation, major and minor axis lengths, etc.) under shear and silencing were obtained using our program (electronic supplementary material, information). Vector control and cells with ROCK–shRNA had initial adaptation responses owing to flow followed by gradual returning changes. However, MSCs with FAK–shRNA had impaired responses in cell morphology adaptations under flow, as was similarly seen for the static case (figure 4*c*). It is notable the morphology recovering tendency after initial adaptation appeared to be less pronounced at higher shear stresses of FF15 and FF25 (e.g. area, circularity and major axis length in electronic supplementary material, figures S9, S10, S12). The orientation angle (electronic supplementary material, figure S11), an angle between the cell major axis and the flow direction, was smaller for sheared cells relative to the static counterpart for all conditions tested.

4. Discussion

The study of MSC migration under fluid flow may have significant implications in cell therapy and regenerative medicine. The homing ability of MSCs to damaged tissues, tumours, myocardial infarction and sites of inflammation associated with autoimmune disorders makes MSCs a natural vehicle for cell-based therapy [2]. While the systemic or local delivery of MSCs has been attempted to treat these diseases, the process of MSC translocation and the role of flow shear in particular are not well understood. Improvements to cell injection therapy could be made if the cell migration to damaged sites is better understood. MSC homing depends on migration through a vessel under flow, adhesion to the vessel wall and intrusion through endothelial layer. The success of these processes may be affected by the shear stress and cell mechanotransduction determined by molecular sensors, such as FAK and ROCK, in addition to traditional chemoattractants and related biochemical signalling. This study could also improve tissue engineering scaffold and perfusion bioreactor design. Tissue engineering suffers from low cell invasion into the scaffold. Knowing the effect of bioreactor flow on cell invasion could greatly improve engineered tissue outcomes. Studies have attempted to modulate MSC migration capability. For example, MSCs manipulated to express CXCR4 receptor could be forced to home to the myocardial infarction for heart repair [22]. MSC homing to damaged bone tissue increased with increasing integrin α4 expression [23]. However, the role of flow shear mechanical milieus in MSC migration has seldom been investigated.

We developed methods that significantly extend the capability and power of other open source cell tracking software such as the plugins included in FIJI [7] and TLA [8]. Our program for processing the tracks and morphologies of the cells greatly reduces the amount of time and work required to extract data from the multiple experimental conditions and replicates. Some software (TLA, MTrack2, and TrackMate in FIJI) has adequate segmentation or tracking capabilities but limited post-processing tools. Our scripts allow easy visualization of the entire dataset and enable any migration and morphology parameters to be plotted, compared with parameters from other experimental groups and statistically tested with ANOVA at any time points. Most of the plots shown in this paper were taken directly from the output of our scripts. Our methods were developed to be adaptable and expandable to allow the addition of tracking and morphology measurements not currently implemented. The current scripts process the output files from TLA and process the morphology data from audio video interleave files. The scripts can also process the output files from the MTrack2 plugin and other similar formats, and can easily be extended to accept data in other formats.

We observed that MSCs actively participated in directed crawling migration under flow shear. Our study focused on the crawling motion and did not attempt to quantify migration by other modes such as tethering or rolling [24]. We noted that very few cells under flow sometimes detached with long tethers, at times remaining connected for a couple of minutes. It is possible that these tethering cells re-attempted to participate in the migration. However, the chance of re-attachment may have been minimized as the glass slides used for flow assays were not functionalized with cell-adhesive molecules such as Arg–Gly–Asp ligands. All of the tracking and calculations were set only for the crawling cells.

The cells migrated following the flow direction and the trend became stronger with increasing shear stress magnitude (figures 2 and 3). It is remarkable that these results on MSCs are in contrast with the migration behaviour of other autonomous cells such as leucocytes which tend to be arrested more when rolling under high flow shear [25] and some cancer cells which are inclined to migrate against the interstitial flow [26]. Although not clear at this stage, potential differences in the migration mode, flow regimen and cell type may bring about such differences. It may also be notable that the cells in the FF2 group had relatively greater arrest coefficient (figure 3*c*) and no net migration against the flow (figure 2*e*), although both of these results were not statistically significant. This may at least suggest that at some lower shear stress range MSCs may stop longer and do not move either following or against the flow. Further investigation of MSC migration at varying shear stresses may reveal shear levels leading to MSC arrest. Another thing to note is the lack of long-term differences in cell speed with respect to shear stress level (figure 3*d*,*e*, after

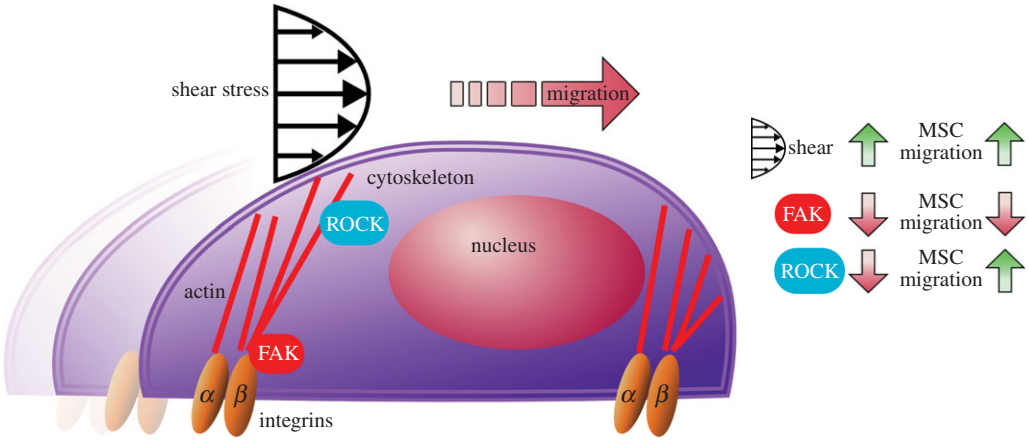

Figure 6. MSC migration under flow changes in a shear stress magnitude-dependent manner and is differentially affected by FAK and ROCK silencing. With increasing shear stress, MSC migrated further with straighter paths. FAK silencing decreased RMS displacement and motility coefficient, whereas ROCK silencing stimulated cell migration under flow shear. This may suggest different roles for focal adhesion signalling via FAK and cytoskeletal tension signalling via ROCK in the flow shear induction of MSC migration.

about 10 min), regardless of marked differences in cumulative migration data. As commented earlier, various cell reactions to flow shear, as outlined through our methods with multi-aspect migration parameters (displacement, confinement ratio, arrest coefficient, speed, time migrating with or against the flow or more collectively as RMS displacement and motility coefficient or MSD), contribute together to form the observed cell migration behaviour.

Silencing the key focal adhesion mechanosensor, FAK, suppressed MSC migration for both static and flow conditions (figures 4 and 5), indicating that FAK is necessary for MSC migration. The decreased migration by FAK–shRNA may be due to the difficulty in focal adhesion turnover. It was reported for endothelial cells under flow shear that FAK was recruited to form new focal adhesions at the leading edge of the migration and the stress fibres connected to these new focal adhesions were more stable relative to those at other sites [27]. The focal adhesion turnover would be limited in MSCs with FAK–shRNA, reducing the capability to create new attachment sites required for migration. In addition, FAK silencing reduced morphology adaptation responses, as assessed by limited changes in area and circularity during the time lapse period for both static (figure 4*c*) and flow conditions (electronic supplementary material, information). The lack of morphology adaptation by FAK knockdown is consistent with the reported role of FAK as a general cell adhesion mechanosensor [28].

The other key mechanosensing component, cytoskeleton, may contribute differently to MSC migration. Silencing of ROCK, which regulates cytoskeleton formation and cell tension, actually caused increased migration tendencies in both static and sheared conditions (figures 4 and 5). Our results are in line with other studies that showed enhanced migration under ROCK inhibition, for example increased trans-endothelial migration of MSCs [16], promoted migration in neural cells [17] and restored motility in γ-actin-knockdown cells [29]. However, all of these studies only dealt with static culture. Our study is the first study, to the best of our knowledge, to show that ROCK–shRNA facilitates MSC migration under mechanical milieus such as fluid shear. It has been proposed for static culture that blocking ROCK diminishes cytoskeletal tension which may lower the resistance to remodelling during migration [16,17]. A similar mechanism may be applied for the flow shear situation. On the other hand, some study proposed that ROCK may be less important for cell migration (but under static culture). For leucocytes, cell migration via lamellipodia formation at the leading edge of the cell is driven by actin polymerization via Rac, whereas the contraction via RhoA–ROCK may act primarily at the trailing edge [30]. While this report is for static culture, of particular interest for further study under flow will be the Rac pathway. Rac is part of the Rho family of small GTPases that regulate the mode of cell migration by controlling cytoskeletal protrusion and contraction. Rac is involved in many cellular functions, including polarization, cell adhesion and migration [31]. The Rac and Rho pathways are generally antagonistic with complex spatio-temporal regulation, which is poorly understood to date [32]. Because it was shown for leucocytes under static culture that Rac plays a role associated with cytoskeletal protrusions at the leading edge of the cell migration [30], evaluating the role of Rac in MSC migration under physiologically relevant shear stress will greatly broaden our understanding of the underlying molecular mechanisms in MSC migration and homing.

Combining our results, silencing FAK (focal adhesion signalling) is inhibitory of MSC migration, whereas silencing ROCK (cell tension signalling) is stimulatory. A possible explanation may include that FAK inhibition could be tied to an increase in Rho [33], an upstream effector of ROCK, which increases cytoskeletal tension therefore decreasing the cytoskeletal adjustment capability required for migration. Additionally, unlike FAK–shRNA, ROCK silencing appeared not to impair cell morphology adaptation capability. In another group's study using Y-27632, which inhibits both ROCK-I and ROCK-II, MSCs showed suppressed morphology adaptation response under fluid flow [4]. The comparison may suggest a separate role of ROCK-I and ROCK-II in cell shaping under flow shear (remember that our shRNA specifically knocked down ROCK-I). Cell areas for FAK–shRNA and ROCK–shRNA were, in general, smaller than that of the vector control (figure 4*b*,*c*; especially after sufficient adaptation–recovery period or after about an hour). A small cell area with ROCK–shRNA was also observed in our recent study of MSC alignment on nanofibre substrates [19].

Future studies would benefit from investigating the combined effects of fluid flow regimens (shear stress magnitude, steady versus pulsatile versus oscillatory, frequency, duration,

rest period, macro flow versus microfluidic flow, two- versus three-dimensional), the presence of chemoattractants and the other molecular manipulations (inhibition or overexpression) on MSC mobility. As discussed above, this will practically improve strategies of cell injection therapy. Examining the migration of MSCs under flow on or through biomaterials would also advance the strategies used in tissue engineering scaffolds and bioreactors. Definitely in-depth assessment of intra- and intercellular signalling pathways of the migrating MSCs owing to flow shear would provide insights into the cellular migration processes and may reveal therapeutic targets to manipulate for controlling MSC migration efficiency.

In conclusion, we developed methods for efficiently and accurately tracking, measuring and processing cell migration and morphology. The methods built on open source peer-reviewed software and increased the ease and speed of processing the results. Using these methods, we found that flow shear stress level has a significant influence on MSC migration. The total and RMS displacements, confinement ratio, motility coefficient, number of cells migrating with the flow and time of cell migrating with the flow had an increasing trend with increasing shear stress. Silencing FAK and ROCK had opposing effects on MSC migration, which may highlight the unique role of these molecular sensors each representing focal adhesion and cytoskeletal tension signalling. MSCs with interfered FAK had decreased motility coefficient in both static and flow conditions, whereas ROCK silencing stimulated MSC migration especially under the flow shear condition. FAK-silencing reduced morphology adaptation capability while ROCK-silencing did not. A summary diagram of our findings focusing on migration is illustrated in figure 6. The results obtained using our tracking and analysing methods may advance strategies of cell therapy and tissue engineering.

Funding statement. The authors thank the funding support from NSF CAREER (1351570), AHA Scientist Development Grant (12SDG12030109), Osteology Foundation Grant (12-006), and Nebraska Research Initiative (all to JYL).

Competing financial interests. The authors declare no competing financial interests.

References

1. Dittmar T, Entschladen F. 2013 Migratory properties of mesenchymal stem cells. In *Mesenchymal stem cells: basics and clinical application I* (eds B Weyand, M Dominici, R Hass, R Jacobs, C Kasper), pp. 117–136. Berlin, Germany: Springer.
2. Kang SK, Shin IS, Ko MS, Jo JY, Ra JC. 2012 Journey of mesenchymal stem cells for homing: strategies to enhance efficacy and safety of stem cell therapy. *Stem Cells Int.* **2012**, 1–11. (doi:10.1155/2012/342968)
3. Malek AM, Alper SL, Izumo S. 1999 Hemodynamic shear stress and its role in atherosclerosis. *JAMA* **282**, 2035–2042. (doi:10.1001/jama.282.21.2035)
4. Zheng W, Xie Y, Zhang W, Wang D, Ma W, Wang Z, Jiang X. 2012 Fluid flow stress induced contraction and re-spread of mesenchymal stem cells: a microfluidic study. *Integr. Biol.* **4**, 1102–1111. (doi:10.1039/C2IB20094E)
5. Chamberlain G, Smith H, Rainger GE, Middleton J. 2011 Mesenchymal stem cells exhibit firm adhesion, crawling, spreading and transmigration across aortic endothelial cells: effects of chemokines and shear. *PLoS ONE* **6**, e25663. (doi:10.1371/journal.pone.0025663)
6. Maijenburg MW, van der Schoot CE, Voermans C. 2012 Mesenchymal stromal cell migration: possibilities to improve cellular therapy. *Stem Cells Dev.* **21**, 19–29. (doi:10.1089/scd.2011.0270)
7. Schindelin J *et al*. 2012 Fiji: an open-source platform for biological-image analysis. *Nat. Methods* **9**, 676–682. (doi:10.1038/nmeth.2019)
8. Huth J, Buchholz M, Kraus JM, Schmucker M, von Wichert G, Krndija D, Seufferlein T, Gress TM, Kestler HA. 2010 Significantly improved precision of cell migration analysis in time-lapse video microscopy through use of a fully automated tracking system. *BMC Cell Biol.* **11**, 24. (doi:10.1186/1471-2121-11-24)
9. Jin T. 2013 Gradient sensing during chemotaxis. *Curr. Opin. Cell Biol.* **25**, 532–537. (doi:10.1016/j.ceb.2013.06.007)
10. Rodriguez LL, Schneider IC. 2013 Directed cell migration in multi-cue environments. *Integr. Biol.* **5**, 1306–1323. (doi:10.1039/C3IB40137E)
11. Riehl BD, Lim JY. 2012 Macro and microfluidic flows for skeletal regenerative medicine. *Cells* **1**, 1225–1245. (doi:10.3390/cells1041225)
12. Tomakidi P, Schulz S, Proksch S, Weber W, Steinberg T. 2014 Focal adhesion kinase (FAK) perspectives in mechanobiology: implications for cell behaviour. *Cell Tissue Res.* **357**, 515–526. (doi:10.1007/s00441-014-1945-2)
13. Peng X, Guan J-L. 2011 Focal adhesion kinase: from *in vitro* studies to functional analyses *in vivo*. *Curr. Protein Pept. Sci.* **12**, 52–67. (doi:10.2174/138920311795659452)
14. Golubovskaya VM. 2010 Focal adhesion kinase as a cancer therapy target. *Anticancer Agents Med. Chem.* **10**, 735–741. (doi:10.2174/1871520 10794728648)
15. McBeath R, Pirone DM, Nelson CM, Bhadriraju K, Chen CS. 2004 Cell shape, cytoskeletal tension, and RhoA regulate stem cell lineage commitment. *Dev. Cell* **6**, 483–495. (doi:10.1016/S1534-5807(04)00075-9)
16. Lin M-N, Shang D-S, Sun W, Li B, Xu X, Fang W-G, Zhao W-D, Cao L, Chen Y-H. 2013 Involvement of PI3K and ROCK signaling pathways in migration of bone marrow-derived mesenchymal stem cells through human brain microvascular endothelial cell monolayers. *Brain Res.* **1513**, 1–8. (doi:10.1016/j.brainres.2013.03.035)
17. Leong SY, Faux CH, Turbic A, Dixon KJ, Turnley AM. 2011 The Rho kinase pathway regulates mouse adult neural precursor cell migration. *Stem Cells Dayt. Ohio* **29**, 332–343. (doi:10.1002/stem.577)
18. Lee JS, Ha L, Kwon IK, Lim JY. 2013 The role of focal adhesion kinase in BMP4 induction of mesenchymal stem cell adipogenesis. *Biochem. Biophys. Res. Commun.* **435**, 696–701. (doi:10.1016/j.bbrc.2013.05.045)
19. Andalib MN, Lee JS, Ha L, Dzenis Y, Lim JY. 2013 The role of RhoA kinase (ROCK) in cell alignment on nanofibers. *Acta Biomater.* **9**, 7737–7745. (doi:10.1016/j.actbio.2013.04.013)
20. Rao DD, Vorhies JS, Senzer N, Nemunaitis J. 2009 siRNA vs. shRNA: similarities and differences. *Adv. Drug Deliv. Rev.* **61**, 746–759. (doi:10.1016/j.addr.2009.04.004)
21. Sumen C, Mempel TR, Mazo IB, von Andrian UH. 2004 Intravital microscopy: visualizing immunity in context. *Immunity* **21**, 315–329. (doi:10.1016/j.immuni.2004.08.006)
22. Cheng Z *et al*. 2008 Targeted migration of mesenchymal stem cells modified with CXCR4 gene to infarcted myocardium improves cardiac performance. *Mol. Ther.* **16**, 571–579. (doi:10.1038/sj.mt.6300374)
23. Kumar S, Ponnazhagan S. 2007 Bone homing of mesenchymal stem cells by ectopic α4 integrin expression. *FASEB J.* **21**, 3917–3927. (doi:10.1096/fj.07-8275com)
24. Rüster B, Göttig S, Ludwig RJ, Bistrian R, Müller S, Seifried E, Gille J, Henschler R. 2006 Mesenchymal stem cells display coordinated rolling and adhesion behavior on endothelial cells. *Blood* **108**, 3938–3944. (doi:10.1182/blood-2006-05-025098)
25. Sundd P, Pospieszalska MK, Cheung LS-L, Konstantopoulos K, Ley K. 2011 Biomechanics of leukocyte rolling. *Biorheology* **48**, 1–35. (doi:10.3233/BIR-2011-0579)
26. Polacheck WJ, Charest JL, Kamm RD. 2011 Interstitial flow influences direction of tumor cell

migration through competing mechanisms. *Proc. Natl Acad. Sci. USA* **108**, 11 115–11 120. (doi:10.1073/pnas.1103581108)

27. Li S, Butler P, Wang Y, Hu Y, Han DC, Usami S, Guan J-L, Chien S. 2002 The role of the dynamics of focal adhesion kinase in the mechanotaxis of endothelial cells. *Proc. Natl Acad. Sci. USA* **99**, 3546–3551. (doi:10.1073/pnas.052018099)
28. Holle AW, Engler AJ. 2011 More than a feeling: discovering, understanding, and influencing mechanosensing pathways. *Curr. Opin. Biotechnol.* **22**, 648–654. (doi:10.1016/j.copbio.2011.04.007)
29. Shum MSY, Pasquier E, Po'uha ST, O'Neill GM, Chaponnier C, Gunning PW, Kavallaris M. 2011 γ-Actin regulates cell migration and modulates the ROCK signaling pathway. *FASEB J.* **25**, 4423–4433. (doi:10.1096/fj.11-185447)
30. Biro M, Munoz MA, Weninger W. 2014 Targeting Rho-GTPases in immune cell migration and inflammation. *Br. J. Pharmacol.* **171**, 5491–5506. (doi:10.1111/bph.12658)
31. Murali A, Rajalingam K. 2014 Small Rho GTPases in the control of cell shape and mobility. *Cell. Mol. Life Sci.* **71**, 1703–1721. (doi:10.1007/s00018-013-1519-6)
32. Sadok A, Marshall CJ. 2014 Rho GTPases. *Small GTPases* **5**, e29710. (doi:10.4161/sgtp.29710)
33. Mierke CT. 2013 The role of focal adhesion kinase in the regulation of cellular mechanical properties. *Phys. Biol.* **10**, 065005. (doi:10.1088/1478-3975/10/6/065005)